Temperature-controlled martensitic phase transformations in a model NiAl alloy

N. P. Lazarev[a)]
NSC Kharkov Institute of Physics and Technology, 61108 Kharkov, Ukraine

C. Abromeit
Hahn-Meitner-Institut Berlin GmbH, 14109 Berlin, Germany

R. Schäublin
Centre de Recherche en Physique de Plasma, École Polytechnique Fédérale de Lausanne, 5232 Villigen-PSI, Switzerland

R. Gotthardt
Institut de Physique de la Matière Complexe, École Polytechnique Fédérale de Lausanne, 1015 Lausanne, Switzerland

(Received 10 May 2006; accepted 17 July 2006; published online 26 September 2006)

Reversible martensitic phase transformations in a partially disordered Ni–Al alloy within the composition range from 60 to 65 at. % of Ni are investigated using molecular dynamics simulation. During a complete temperature cycle a wide hysteresis in enthalpy, volume, and shape of the simulated crystals is observed. The temperature T_0 of the phase transformation is found from the calculated free energy evolution. To investigate the atomic-scale development during the phase transformation a local order parameter is defined which is based on a combined method of Voronoy tessellation [J. Reine Angew. Math. **134**, 198 (1908)] with common-neighbor analysis. This local order parameter allows us to get a detailed localized picture of nucleation and growth of the new phases. Both homogeneous formation of the new phase and heterogeneous nucleation are observed. The velocity of new phase growth front is estimated. © *2006 American Institute of Physics*.
[DOI: 10.1063/1.2352811]

I. INTRODUCTION

Already 35 years ago the thermoelastic behavior in Ni–Al system has been studied. The relationship between composition and the appearance of the shape memory effect was established.[1,2] Since then the thermally and mechanically induced martensitic phase transformations (MPTs) in NiAl shape memory alloy were investigated experimentally and theoretically in detail. In composition ranges from 60 to 65 at. % of Ni this alloy exhibits reversible martensitic transformations between a high temperature partially disordered B2 structure and a low temperature martensite phase with tetragonal $L1_0$ close-packed structure (fct). The evolution of the transformation depends strongly on the microstructure of the phases, which includes dislocation arrays, micrograin heterogeneities, and precipitates of secondary phases.

The MPTs in general are divided in two steps, namely, nucleation and growth of the new phase. Since the nucleation process cannot be experimentally observed directly because of the extremely short transition times in the picoseconds range, simulation is still the most appropriate technique to investigate it. More precisely, the nondiffusional nature of austenite-martensite transition implies that the phase transformation occurs in length and time scales that are well best suited for the application of the molecular dynamics (MD) simulation technique.[3] However, the validity of MD simulations to properties of real systems substantially depends on the correctness of the used interatomic potentials. In this respect quantum mechanical calculations are most accurate, but they are restricted to relatively small systems, hundreds of atoms at most, and short simulated times, picoseconds at most. During the phase transformation the fluctuations in thermodynamic quantities increase to such an extent that the size of the model system has to be adapted in order to avoid sampling problems. For example, the crystallization kinetics starting from the liquid is fairly sensitive to the size of system up to millions of atoms.[4] Specifically, for MPT, the phenomena such as soft phonon modes development, nucleation, and coherent propagation of a new phase involve a fairly large number of atoms. Therefore we use classical MD with empirical potentials.

For the Ni–Al system several empirical many-body embedded atom method (EAM) potentials were developed.[5–8] Its martensitic phase transformations could be reproduced.[8–13] In order to get more insight in the local transformation details we perform MD simulation of temperature-controlled MPTs. The paper is organized as follows. The simulation procedure is formulated in the following section. Temperature dependences of the enthalpy and the shape of simulated box, radial distribution functions for austenite and martensite phases, atomic displacements during MPTs, and composition dependence of transformation temperatures are presented. Next we define a local order parameter allowing to trace the development of MPTs at the atomic scale. A thermodynamic description of the free energy evolution dur-

[a)]Electronic mail: n.lazarev@kipt.kharkov.ua

ing transformations is given in the harmonic approximation for entropy. In order to study characteristics of heterogeneous nucleation and unconstrained propagation of new phases we consider finite-size systems with free external surface. The effect of surface reconstruction on MPTs is revealed. The role of composition ordering is studied in a Ni_5Al_3 alloy.

II. SIMULATION METHOD

A conventional molecular dynamics computer simulation technique[3] is used in this study. We apply the EAM potential for NiAl system developed by Farkas *et al.*[6] Originating from force-field of Voter and Chen,[5] the potential of Farkas *et al.* was specially designed for B2 NiAl and martensitic phases by refitting the Ni–Al mixed bond while keeping the interactions Ni–Ni and Al–Al, as well as the embedding electronic density functions of Ref. 5. Recently this potential has been used for the simulations of the effects of defects on martensite nucleation.[12] Here we note that Table I in Ref. 6 contains a misprint. The values of A and B in this table have to be exchanged. We tried to simulate MPT in NiAl with other potentials, in particular, the ones of Voter and Chen[5] and Mishin *et al.*[7] However, the potential of Farkas *et al.* was found to be the most appropriate to achieve the goals of this study.

The initial structure of NiAl alloy follows an ordered B2 cubic lattice, with the main axes as.[1, 0, 0,], [0, 1, 0,], and [0, 0, 1,]. Since the transformation into martensite phase is usually related to the development of instabilities in the bcc lattice in the closest packing direction $[1,1,1]_{bcc}$, some control runs were carried out with the initial structure being rotated in such a way that the main axes of the simulation cell correspond to the crystallographic directions [1, 1, 1,], $[1,\bar{1},0]$, and $[\bar{1},\bar{1},2]$. In all simulated approaches the common features of transformations were found to be quite similar. Some arguments for the favorable choice of the main axes are discussed in Ref. 14.

The preparation of the partially disordered binary alloy is performed according to Ref. 10. To summarize, an initially compositionally ordered B2 structure is modified by the replacement of randomly chosen Al atoms on the Al sublattice by Ni atoms in accordance with the corresponding composition ratio.

For the simulation of infinite crystals rectangular boxes containing from 10^3 to 10^6 atoms with periodic boundary conditions are used. The method of Berendsen *et al.*[15] of constant temperature and constant stress dynamics is employed. The box sizes L_x, L_y, and L_z are independently varied during the simulations in order to keep zero normal stresses on each of the box faces. Such independent change of the box dimensions makes it possible to follow the shape change during MPT. The relaxation constants were chosen as $\tau_T = 2-4$ ps, for the coupling to an external thermal bath, and as $\tau_S = 1-3$ ps, for constant stress dynamics.

The samples for the simulation of finite-size effects are prepared as follows. Out of an "infinite" crystal we choose a spherical region with a *free* external surface. To obtain the reproducible results the samples are annealed at the temperature of about 1200 K until the surface structure becomes stable. At such temperature almost no bulk diffusion is observed.

Unlike simulations with periodic boundary conditions where the simulation cell is fixed, a system with free external surface is unfixed in space. Additional efforts are made to prevent undesirable drift and rotation of the samples due to accumulation of computational errors. Both total momentum, $\mathbf{P}=\Sigma_i m_i \mathbf{v}_i$, and the angular momentum, $\mathbf{L}=\Sigma_i m_i \mathbf{r}_i \times \mathbf{v}_i$, are set to zero every 100–500 MD steps, where m_i, $\mathbf{r}_i$, and $\mathbf{v}_i$ are the mass, the coordinate, and the velocity of i atom, respectively.

The equations of motion are numerically integrated by a velocity Verlet algorithm with a time step of $\Delta t = 2 \times 10^{-15}$ s. The chosen value Δt is about 20–60 times less than characteristic periods of atom vibrations. This makes the simulation stable.

Structure properties of the alloy are investigated by means of pair radial distribution functions (RDFs), the common-neighbor analysis (CNA) method,[16] and Voronoy tessellation method.[17,18] Before the structure examination, in order to exclude the influence of atomic thermal oscillations we obtain the structural configurations corresponding to atomic potential energy minima. They determine the inherent structure configurations.[19] We use the simple variant of quickest descent method. At a given time we make a copy of our system and perform 10^2-10^3 usual MD steps setting to zero atom velocities at each step, and a time step being as large as possible to decrease the potential energy of the system.

III. GENERAL ASPECTS OF REVERSIBLE MPTS IN PERFECT CRYSTAL

A. Hysteresis

A necessary feature of MPT is the strict reversibility of the structural properties of the alloy at the end of complete temperature or stress cycle, corresponding to austenite $A \rightarrow$ martensite $M \rightarrow$ austenite A. The hysteresis of the thermodynamics properties is determined by two factors: (a) the kinetic processes of the nucleation of the new phases, i.e., a temperature rate dependent MPT, and (b) the heterogeneity of the alloy, i.e., a temperature rate independent MPT.

Most of the previous MD simulations of MPT were focused on the heterogeneous nucleation of the new phase at various extended lattice defects such as external surfaces, dislocations, grain boundaries, etc., see, e.g., Refs. 12 and 20 and references therein. Here we study a reversible MPT in a NiAl alloy which initially does not contain extended defects. Figure 1 shows an example of such transformation hysteresis: the reduced enthalpy-temperature (left) and deformation-temperature (right) relations for a comparatively small sample with Ni–37%Al composition. In this paper the calculated enthalpy was shifted by 4.6 eV which is about the magnitude of cohesive energy in perfect Ni_3Al. The corresponding dependence of volume on temperature was published in Ref. 21. The initial austenite state was prepared at 800 K as described in the previous section. Stepwise cooling

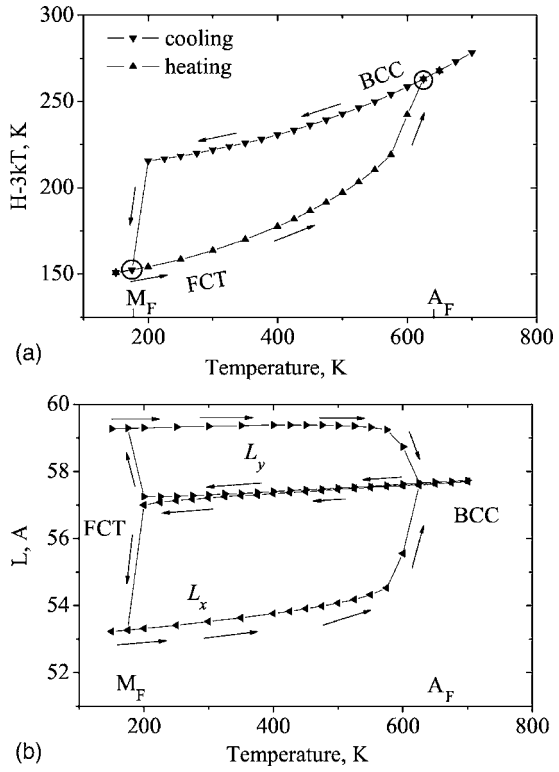

FIG. 1. Temperature dependence of (a) the reduced enthalpy and (b) the dimensions of the simulated box of the Ni–37%Al sample containing 16 000 atoms. At each temperature point depicted by triangle symbols the annealing time is 0.25 ns. Together with a temperature step of 25 K this corresponds to an effective cooling/heating rate of 10^{11} K/s. The lines are drawn as guides for the eyes only.

results in an $A \rightarrow M$ transformation at temperature $M_F = 150$ K and subsequent heating brings the system back to the austenite bcc structure at $A_F = 625$ K.

Transition temperatures M_F and A_F depend on the cooling/heating rates. For a larger rate the hysteresis becomes broader. This effect hints to a kinetic-controlled MPT.

From the other side the hysteresis width essentially depends on defect structure of martensite state. Figure 2 shows two examples of such dependence for different samples. These samples have comparable sizes but differ by structure of the martensitic phase. The first sample (D) contains stable twin faults in martensite state but the second one (P) is found

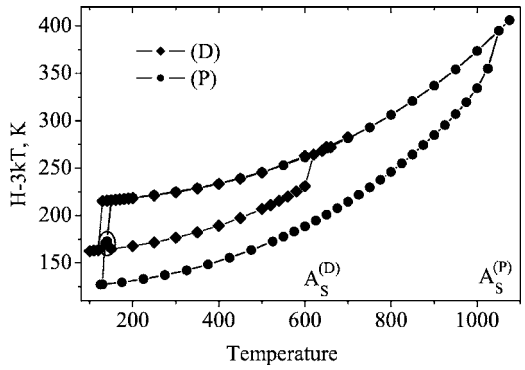

FIG. 2. Hysteretic behavior of different samples at equal composition Ni–37%Al. Samples D and P consist of 69 118 and 65 536 atoms, respectively. The effective cooling/heating rates were about 10^{11} K/s for both samples.

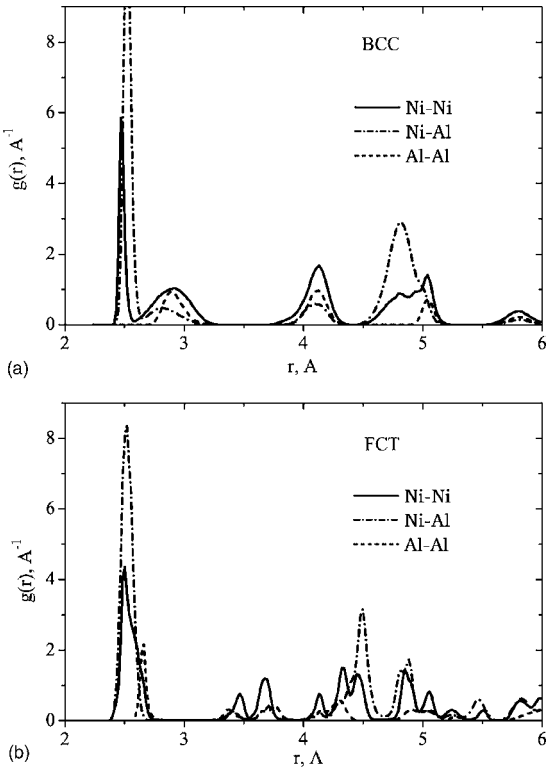

FIG. 3. RDFs of NiAl (a) austenite phase before transformation to martensite, $T = 200$ K, and (b) martensite phase after transformation in Ni–37%Al, $T = 175$ K.

as defect free martensite. One can see that the hysteresis width ΔT_{AM}^H depends on the difference of enthalpies of high-temperature and the low-temperature phases ΔH_{AM} in the vicinity of transition $A \rightarrow M$. For sample D the value of ΔT_{AM}^H amounts to about 450 K and $\Delta H_{AM} \sim 60$ K; for sample P these values are $\Delta T_{AM}^H \sim 850$ K and $\Delta H_{AM} \sim 90$ K.

B. Radial distribution functions

The type of the phase state was determined by the partial RDF,

$$g(r) \propto \frac{1}{4\pi r^2} \left\langle \sum_i \sum_{j \neq i} \delta(r - r_{ij}) \right\rangle, \tag{1}$$

Figure 3 shows RDFs of partially disordered NiAl alloy for the two phase states.

At two temperatures depicted by circles on Fig. 1(a), there is an abrupt change of the enthalpy and of the RDF. However, the transition cycle $A \rightarrow M \rightarrow A$ is reversible as the RDF is recovered for completion of a full cycle and each atom returns back exactly to the initial position of the beginning of the simulation.

C. Atomic displacements

An example of the time dependence of atomic displacements is presented in Fig. 4. The data were taken for P sample which hysteretic history is shown in Fig. 2. The displacement monitoring starts at the point of phase transition $A \rightarrow M$ at $T = 140$ K. Subsequent to the oscillatory increase after about 0.01 ns, the mean square displacement (MSD)

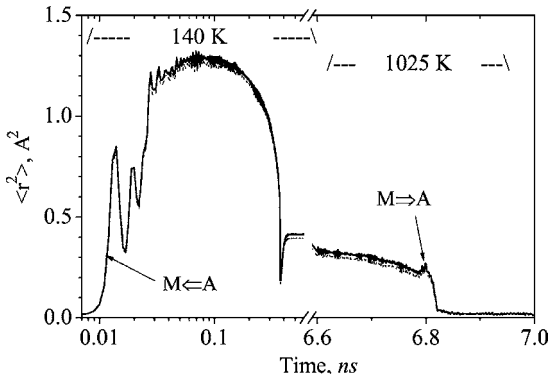

FIG. 4. The time dependence of MSD in NiAl during complete hysteretic cycle shown in Fig. 2 for system P. The solid and dotted lines correspond to Ni and Al components, respectively.

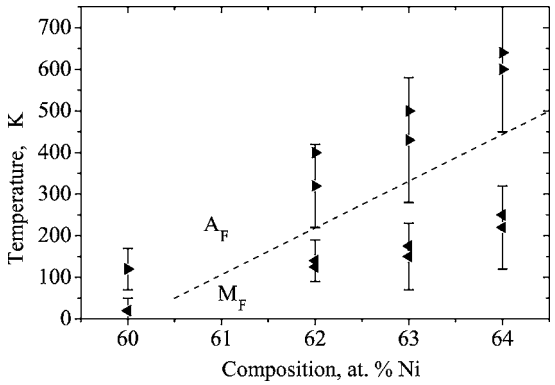

FIG. 5. Composition dependence of NiAl MPT temperatures M_F and A_F. The dashed line shows the experimental data.

amounts to about 1.4 Å^2. Moreover both components Ni and Al drift synchronously, which point to the cooperative movements of atoms during MPT.

The main contribution in MSD is due to the formation of a system of twins which slightly unwrap with respect to each other minimizing the energy of the twin boundaries. In about 0.3 ns the most "thick" twin boundaries are annealed and the formation of almost perfect hcp structure takes place. The dependence after about 6.6 ns of the simulation corresponds to the reverse transition $M \rightarrow A$ at $T=1025$ K. One can see that after some incubation period from 6.6 to 6.8 ns a fast phase transition takes place and MSD reduces to nearly zero. Note that the MSD are presented without thermal oscillations. Thus after the complete simulation cycle of 14 ns or 7×10^7 MD steps including the phase transitions $A \rightarrow M$ and back $M \rightarrow A$ the mean displacement of atoms amounts to 0.1 Å only. This supports the nondiffusional nature of the observed MPTs and verifies indirectly the accuracy of the numerical approaches used.

D. Composition dependence

With decreasing Ni content both temperatures M_F and A_F shift to lower values, whereas increasing Ni content gives higher transition temperatures (see Fig. 5). The order of magnitudes of MPT temperatures appears to be in accordance with the ones experimentally observed for Ni–Al alloy.[22]

In simulations with samples of a Ni concentration below 62% phase transitions $A \rightarrow M$ were not observed in all cases. At the composition Ni–40%Al the transition has only been found in one out of three examples. The temperature of reverse transition $M \rightarrow A$ is highly sensitive to martensite defect structure and can vary over hundreds of degrees depending on specimen size, initial conditions, and treatment history as it can be seen in Fig. 2.

IV. LOCAL ORDER PARAMETER

While the radial distribution function is completely adequate to distinguish the two structural phase states before and after the phase transition, it is insufficient to follow the structure evolution locally. In order to investigate the local character of the transformation we define an appropriate local order parameter which describes the nearby structure symmetry around each atom, i.e., the structural local environment. Our definition of such local order parameter is based on the technique of the CNA.[16] The CNA was initially developed for characterization of highly disordered systems such as liquids and glasses but it also appears to be a useful tool for identification of various defects in crystals (see, e.g., Ref. 24).

According to the CNA each pair of atoms $A-B$ (bond) is attributed to four indexes: $lijk$. The first index l is equal to 1 if A and B are neighbors and l is equal to 0 otherwise. The second index i gives the number of common neighbors of A and B. The next index j is the number of common bonds between common neighbors and k is the longest continuous chain formed by bonds between common neighbors. One can see that CNA method is essentially supported by the concept of "neighbor atom." The traditional approach for the nearest neighbor definition uses a simple criterion: two atoms are regarded as the nearest neighbors if they are within a certain cutoff distance r_c from each other. Usually r_c is taken from the origin to the first minimum of the radial distribution function. For example, as it follows from Fig. 3 the optimal choice for r_c would be 3.5 A for bcc lattice and 3.0 Å for hcp one. Such criterion of neighbor selection for CNA provides a good stability against small deviation of atomic positions from equilibrium and gives acceptable results for homogeneous systems. However, this traditional approach is not useful in case of an essential structure change as it takes place during the phase transformations as treated here. One of the possible ways of generalization of this method on heterogeneous systems could be dissection of the whole system into subdomains, construction of local RDFs, and the relevant choice of $r_c^{(i)}$ for each of i subdomain. However, thus it is necessary to introduce the size of an averaging subdomain as an optional parameter which is inappropriate. Also such approach does not allow us to explore abrupt changes of structure which occur, e.g., on interphase boundaries.

To overcome these difficulties we propose a more straightforward approach, based on the space tessellation by Voronoy polyhedra[17] according to the description.[18] Voronoy construction generalizes the conception of a Wigner-Seitz cell to arbitrary particle ensemble. We consider that two atoms are neighbors if their Voronoy polyhedra share a common face. With this definition, bcc and fcc lattices have co-

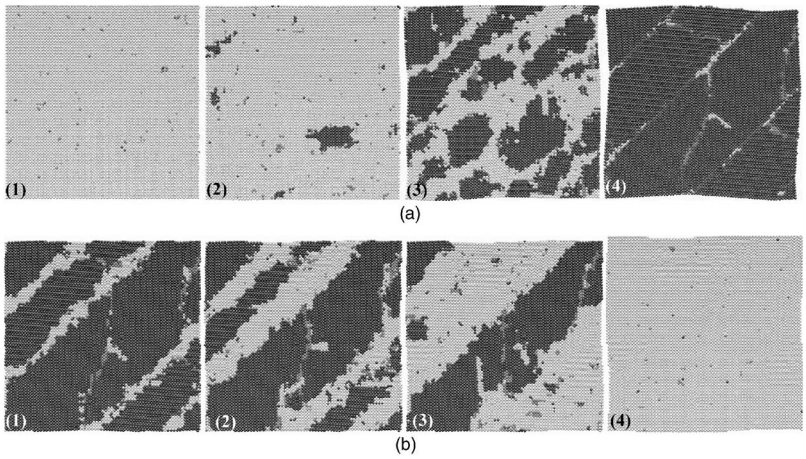

FIG. 6. (a) Homogeneous $A \rightarrow M$ transformation: (1) fragment of an initial state of overcooled austenite, (2) homogeneous nucleation of martensite nuclei, (3) twinning structure formation, and (4) final martensite state after the transformation. Atoms in bcc environment depicted as gray, in fcc and hcp one as black, and others as deep-gray. Temperature: $T=115$ K and number of atoms in the simulated box: $N=245\,000$. (b) Heterogeneous $M \rightarrow A$ transformation: (1) austenite phase starts to grow at the twin boundaries, (2) and (3) linear growth of austenite in martensite, and (4) final austenite state after the transformation. The same sample as in the Fig. 3(a) but at the temperature $T=650$ K.

ordination numbers of 14 and 12, respectively. It is known that Voronoy polyhedra associated with close-packed structures such as perfect fcc and hcp environments are unstable against small fluctuations of atomic coordinates.[25] Specifically, several fluctuating faces appear in addition to the 12 regular faces. For a Ni–Al alloy the partial compositional disorder and tetragonality of martensitic phase make analysis even more complicated. In order to select the stable topological constructions we use the known technique of Voronoy polyhedron reduction. This can be done by elimination of small edges.[4,25] We use a simpler procedure, namely, the elimination of small faces. After constructing each polyhedron in the usual way we calculate its face areas. If the area of a certain face is less than 20% of the average area of the assigning polyhedron faces then this face is eliminated. Such criterion of face smallness was found as optimal for various structural states of Ni–Al alloy.

At the second step we find the type of each bond by CNA. The type of local environment of each atom σ_i is defined by the set of its bonds. For the phase transformation treated here, we count several predefined types of order in the nearest environment: a perfect bcc if an atom has eight bonds of 1444 type and six bonds of 1666 type, a distorted bcc, i.e., dbcc if an atom has more than ten bonds of 1444 and 1666 types, a perfect fcc if an atom has 12 bonds of 1421 type, a perfect hcp if an atom has six bonds of 1421 type and six bonds of 1422 type, etc. A local order parameter of an i atom σ_i^α is defined by the rule: $\sigma_i^\alpha=1$ if i atom has the local environment of α type and $\sigma_i^\alpha=0$ otherwise, where α is one of the predefined types: bcc, dbcc, fcc, hcp, etc. With this parameter the phase transformation can be followed on an atomic scale showing the time evolution of nucleation, growth, and redistribution of the new phase. The relation to extended lattice defects, inner and outer surfaces, or else can be easily demonstrated.

Each atom can have only one predefined local order according to the definition

$$\sum_\alpha \sigma_i^\alpha = 1. \tag{2}$$

Averaging over all atoms gives the global order parameter,

$$\langle \sigma^\alpha \rangle = \sum_i \sigma_i^\alpha / N. \tag{3}$$

Accordingly the fraction of the austenite phase we define as $\sigma^A=\sigma^{\mathrm{bcc}}+\sigma^{\mathrm{dbcc}}$ and martensitic phase comprises close-packed structures: $\sigma^M=\sigma^{\mathrm{fcc}}+\sigma^{\mathrm{hcp}}+\sigma^{\mathrm{dfcc}}+\sigma^{\mathrm{dhcc}}$. Here and later we use the definition of bcc, fcc, and hcp environments in a sense of CNA method which cannot distinguish topologically equivalent structures such as fcc and FCT. The real crystallographic structure of homogeneous crystalline parts can be refined by standard methods, e.g., by a structure factor calculation.[26]

V. KINETICS

Figures 6(a) and 6(b) illustrate the MPT kinetics from defect-free austenite to twinned martensite and backwards, respectively. Martensite usually results from development of lattice instability on the direction $(1,1,0)_{\mathrm{bcc}}$. At the same time the origin of the martensitic nucleus in system with periodic boundary conditions is accompanied by the distribution of an elastic stress which boosts the multiple, simultaneous formation of new martensitic nuclei [Fig. 6(a) (2)]. The fast-growing variants of martensite meet each other forming twin boundaries. Closely spaced boundaries are annihilated in short time [Fig. 6(a) (3)] and only a few large twins remain in the simulated box [Fig. 6(a) (3)]. The typical size of twins is about 10 nm. The annealed martensite has hcp structure for the most part. Some amount of fcc-ordered atoms found in planar regions. Twin boundaries are observed of two types. The first one contains remnants of austenitic phase with bcc ordering. Such boundaries have width of several atomic sizes, high energy, and they annihilate first of all. The second type of boundaries is characterized by monatomic extensions, a large content of icosahedral order, and a low energy. These boundaries are rather stable and immobile. Both types of twin boundaries are coherent.

In Fig. 7 the evolution of the local order parameters are shown for (a) $A \rightarrow M$ and (b) $M \rightarrow A$ transforms. As it is seen the homogeneous phase transformation needs more time, fluctuations are more prominent and the final martensite structure contains a significant amount of atoms which cannot be attributed neither to A nor to M structure. It is worth

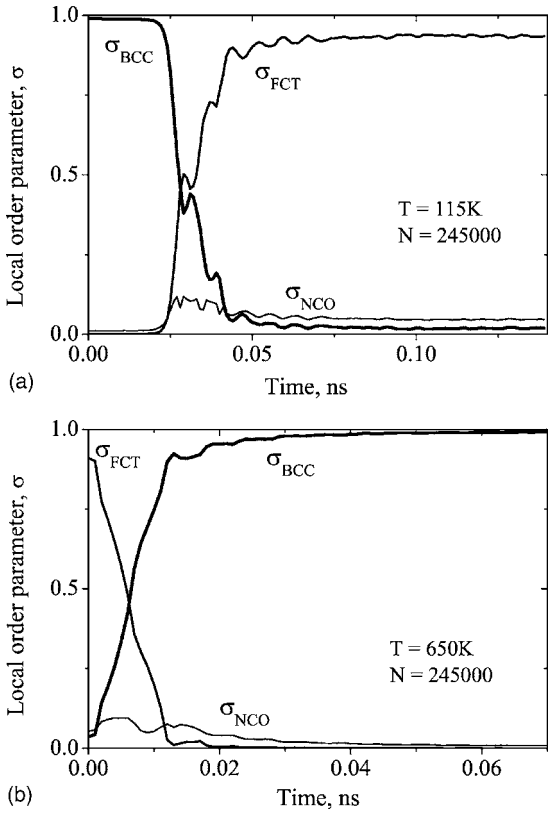

FIG. 7. Evolution of the average local order parameters in NiAl during MPTs for the same system as in Fig. 6. Left: homogeneous MPT from austenite to martensite state and right: heterogeneous reverse transformation from martensite to austenite state.

to note that the final state after the full cycle of transformations is identical to the initial one with the same RDF.

VI. THERMODYNAMICS

The wide hysteresis discovered by the simulations indicates that the system stays in metastable nonequilibrium state for a long time. By decreasing the cooling/heating rate the hysteresis is narrower but the time scale available in the MD method is limited and does not allow to eliminate the wide hysteresis. In order to estimate the temperature of the "true" thermodynamics transition T_0 we use a method based on the calculation of difference of free energies ΔF of two phases.[27] If the difference $\Delta F_{AM}(T)$ is known then the value of T_0 can be determined by the relation

$$\Delta F_{AM}(T_0) = 0. \tag{4}$$

The free energy is defined with the values of enthalpy H and entropy S by

$$F = H - TS. \tag{5}$$

In the MD method, the entropy H can be directly calculated as a sum of potential U and kinetic K energies of all atoms. Entropy is more sophisticated. At constant pressure the thermodynamics relation for entropy is given by

$$S = - \left. \frac{\partial F}{\partial T} \right|_P. \tag{6}$$

By substituting (6) into (5) we obtain for the free energy at constant pressure,

$$\frac{d}{dT}\left(\frac{F}{T}\right) = - \frac{H}{T^2}. \tag{7}$$

Equation (7) is valid both for the martensite state F_M and for the austenitic one F_A. For the difference $\Delta F_{AM} = F_A - F_M$, the solution of Eq. (7) can be written in the form of

$$\frac{\Delta F_{AM}(T)}{T} = \frac{\Delta F_{AM}(T_1)}{T_1} - \int_{T_1}^{T} \frac{\Delta H_{AM}(\tau)}{\tau^2} d\tau. \tag{8}$$

For calculating $\Delta F_{AM}(T)$ the difference of free energies at least at some temperature T_1 has to be known. At sufficiently low temperature, the inharmonic effects can be neglected. We use the expression for the entropy of harmonic system, which takes into account the phonon contribution,[28]

$$S^{\text{har}} = - k_B \sum_{j}^{3N} \ln(\hbar \omega_j / k_B T) + S_0, \tag{9}$$

where k_B is Boltzmann's constant, $\hbar$ is Plank's constant, ω_j is the frequencies of corresponding lattice vibrations, N is the number of atoms in lattice, and S_0 is an appropriate constant. From (9) the difference of entropies reads

$$\Delta S_{AM}^{\text{har}} = - k_B \sum_{j=1}^{3N} \ln(\omega_j^A / \omega_j^M). \tag{10}$$

At the limit of large N this relation becomes

$$\Delta S_{AM}^{\text{har}} = - 3 \int_0^{\infty} \ln(\omega)[g_A(\omega) - g_M(\omega)] d\omega, \tag{11}$$

where $g(\omega)$ is the corresponding spectral density of normal modes.

The easiest way to calculate the spectral density $g(\omega)$ is to use the Fourier transform of the velocity autocorrelation function,[3]

$$A_{VV}(t) = \frac{1}{N} \sum_i \int_0^{\infty} \mathbf{v}_i(\tau) \mathbf{v}_i(\tau + t) d\tau, \tag{12}$$

$$g(\omega) = \frac{1}{\pi} \int_0^{\infty} \cos(\omega t) A_{VV}(t) dt, \tag{13}$$

where $\mathbf{v}_i$ is the velocity of i atom.

Calculating the entropy difference (11) by using the data from Fig. 8, the entropy excess in austenite state of about $0.15 k_B$ per atom as against martensite is obtained. A careful analysis of the spectral densities shows that this excess of entropy is mainly due to the low-frequency region of $g_A(\omega)$.

In martensite the usual dependence $g(\omega) \sim \omega^2$ is observed in the low-frequency region up to the frequencies of about 50 THz. For the austenite phase the quadratic dependence of $g_A(\omega)$ takes place up to the frequencies of about 5 THz only, following by a nearly linear increase, $g(\omega) \sim \omega$. It can be assumed that this is due to the soft modes appearing in the austenite phase.[29] In Fig. 9(a) we plot the difference of enthalpies that is calculated by the data in Fig. 2. The upper curve corresponds to the specimen with the wider hysteresis.

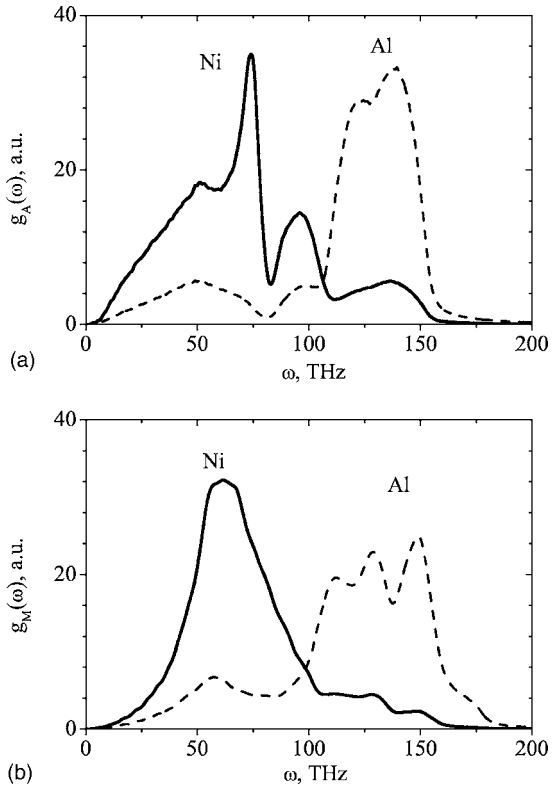

FIG. 8. Spectral densities of normal modes of Ni–37%Al in (a) austenite and (b) martensite states. Solid and dashed lines depict contribution of Ni and Al atoms, respectively.

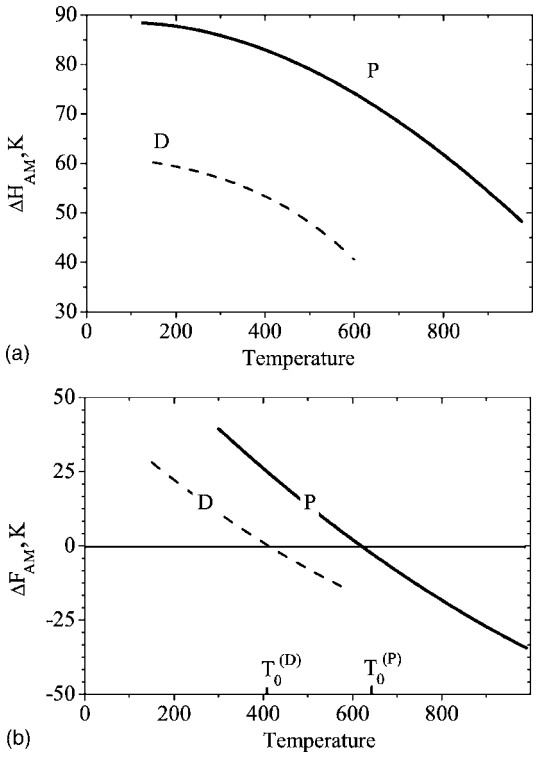

FIG. 9. (a) Enthalpy difference between austenite and martensite states and (b) free energy difference. Solid lines correspond to nearly perfect martensite state P and dashed lines show dependencies for sample with more defective martensite state D.

Figure 9(b) shows the dependencies of calculated free energies. The temperatures of thermodynamic phase transitions $T_0^{(D)}$ and $T_0^{(P)}$ are found in the middle regions of corresponding hysteresis temperature cycles represented in Fig. 2: $T_0^{\alpha} \approx (A_F^{\alpha} - M_F^{\alpha})/2$, α=D and P.

VII. MPT IN FINITE-SIZE SYSTEM: INFLUENCE OF FREE EXTERNAL SURFACE

Periodic boundary conditions allow us to avoid external surface effects which are especially helpful for small systems accessible in MD simulations. At the same time they introduce some undesirable constraints. Note the two aspects: the evolution of MPT occurs usually so fast that it is impossible to adjust the shape of simulation cell by known constant-stress methods as they assume homogeneity of the system. This gives rise to local stresses and leads to formation of large number of twin boundaries.[14] We observe this phenomenon on all samples with sizes exceeding about 10^4 atoms. In addition, the above indicated constrains artificially modify the intrinsic development of a new phase. Hence when we use some constant-stress MD method for simulation of MPT, the conditions take place somewhere in between constant volume and constant stress during fast propagation of the new phase.

The finite-size simulation with free external surface has no such artifacts. Zero external stress is conserved exactly. We use this type of simulation mainly to study peculiarities of an unconstrained propagation of new phases.

Initially, samples are close to spheres in shape. At elevated temperatures the surface atoms become mobile. A characteristic faceting is formed which minimizes the surface energy. Figure 10 shows the influence of surface reconstruction on the MPT development. Simulation starts with bcc structure at 800 K. After cooling to about 75 K the sample undergoes $A \rightarrow M$ transformation. Following heating brings the system back to austenite state at 275 K. At about T_{SR} =950 K the abrupt drop of enthalpy indicates on surface reconstruction. At the second cycle M_F locates at 200 K and A_F at 450 K. Accordingly surface reconstruction gives positive temperature shift of MPT region on 125 K. Further cycling is identical to the second iteration.

Clapp *et al.*[9] have emphasized the role of Ni atoms at the free surface in heterogeneous nucleation of martensite. To check this effect several samples were prepared in which all

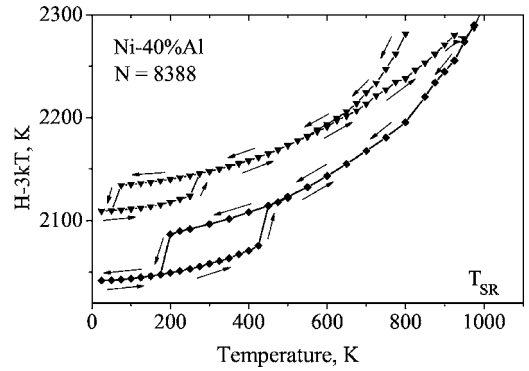

FIG. 10. Temperature dependence of enthalpy at thermocycling. Small triangles depict the fist cycle of cooling/heating and small squares correspond to the second cycle. The annealing time is 0.25 ns at each temperature point.

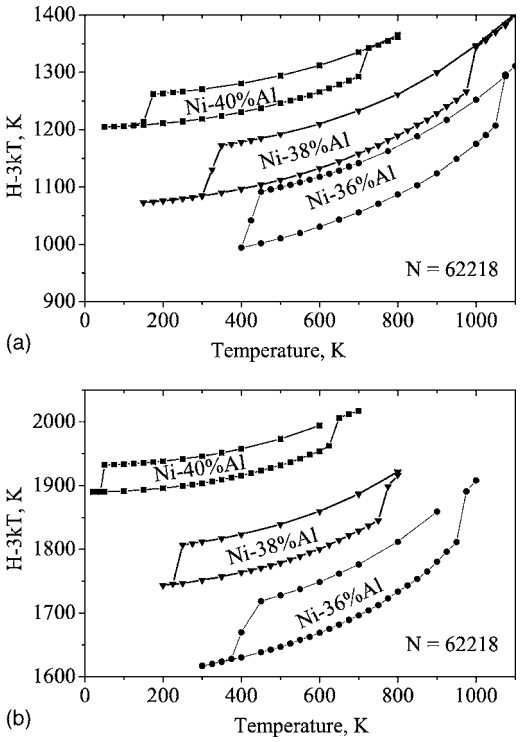

FIG. 11. Temperature dependence of reduced enthalpy for finite-size systems: (a) surface composition is the same as in a bulk, and (b) Al-enriched surface. The annealing times are 0.05 ns at each temperature.

Ni atoms on the surface were substituted by the Al atoms. We qualify surface atoms by a simple rule. For an initially perfect bcc lattice where every bulk atom has 14 nearest neighbors we define surface atoms as atoms having less than 14 neighbors. For perfect close-packed structures, such as fcc or hcp, surface atoms have less than 12 neighbors.

Figure 11 demonstrates the hysteretic behavior of $H(T)$ with respect to MPT at various compositions. Each sample contains 62 218 atoms, corresponding to a diameter of about 11 nm. Note that at this size more than 10% of total number of atoms is situated at the surface. We observe several features: (a) hysteresis width, A_F-M_F, is more narrow than in case of simulations with periodic boundary conditions, (b) free external surface favors to martensite phase, (c) covering of the surface by Al atoms decreases such a preference, and (d) hysteresis width, A_F-M_F, is monotonically increases with enthalpy difference ΔH_{AM}.

A local analysis of phase transformation indicates that the new phase nucleates in the vicinity of an external surface and then rapidly extends to the bulk. Such heterogeneous nucleation is observed for both $A \rightarrow M$ and $M \rightarrow A$ transformations. Due to the unconstrained nature of dynamics and relative small sizes of simulated systems all twin boundaries are annealed in short times. The typical development of local order parameters in time is shown in Fig. 12. After incubation period of about 25 ps the fast phase transformation occurs during $\sim$10 ps. The characteristic plateau in time interval between 37 and 43 ps indicates the contribution of a twin fault which rapidly disappears. The time dependence, shown in Fig. 12, allows us to estimate the velocity of the new

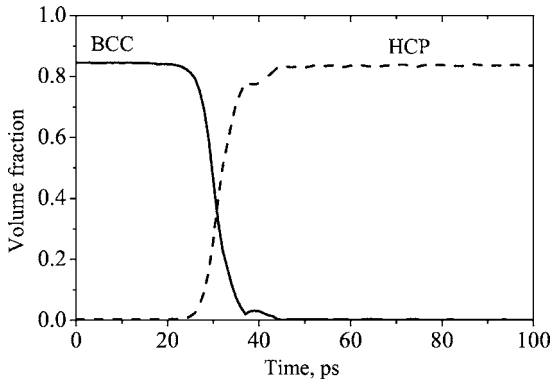

FIG. 12. Evolution of the average local order parameters during transformation $A \rightarrow M$ in Al-enriched Ni–63Al sample containing 130 996 atoms, T=115 K.

martensite phase extension. It is found at about 1×10^4 cm/s, which is only five times slower than sound velocity.

VIII. MPTS IN ORDERED Ni_5AL_3 ALLOY

Up to now we considered a partially disordered binary alloy (PDA). It is interesting to compare the PDA with ordered structure of Ni_5Al_3 which has low temperature bainite (B) phase. The initial structure was prepared according to Ref. 23. Figure 13 shows a simulated behavior of Ni_5Al_3. Several distinctive features are observed.

(a) A complete reversible transformation $B \rightarrow A \rightarrow B$ is possible. It was unclear up to now if the perfect bainite can transform to austenite.

(b) The hysteresis width, A_F-M_F, is broader than in the case of PDA. This can be explained by influence of rectangular shape of simulated box. PDA has larger hexagonality in martensite state. Its squeezing into a rectangular box is entailed by elastic stresses in small systems or the twinning in large ones. In both cases the energy of martensite state increases and consequently the difference ΔH_{AM} decreases. Bainite has nearly equal parts of fcc and hcp types of local orders and can much easily fit the rectangular box.

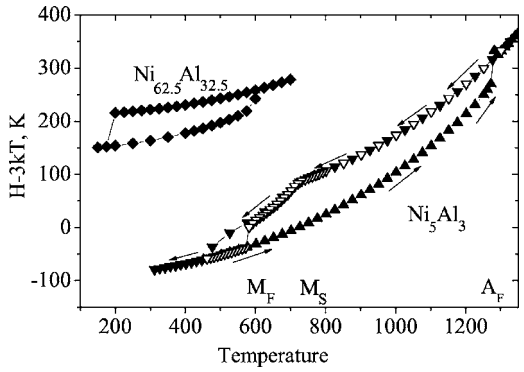

FIG. 13. Temperature dependence of enthalpy of ordered Ni_5Al_3. Number of atoms in cell is N=16 384. Filled triangles show data at heating/cooling and open triangles corresponds to five times slower cooling rate. The annealing times are 0.25 ns at each temperature. For comparison the same dependence for partially disordered alloy with the same composition shown by small squares.

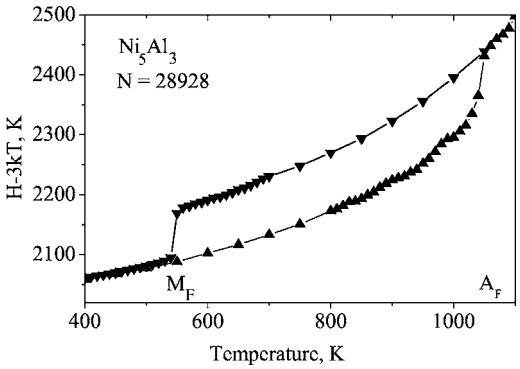

FIG. 14. Temperature dependence of enthalpy of finite-size Ni_5Al_3. The system consists of $N=28\,928$ atoms. Surface was enriched by Al.

(c) Pretransformation phenomena in austenite phase become directly visible on dependence $H(T)$ before transformation $A \rightarrow B$. Clearly seen are two characteristic temperatures M_S and M_F which can be estimated as $M_S=750$ K and M_F is from 475 to 600 K depending on cooling rate. Such type of transformation was never observed for PDA in our simulations.

(d) MPTs in Ni_5Al_3 occur at much higher temperatures: ~400 K difference as compared with PDA.

The behavior of finite-size Ni_5Al_3 ordered system (Fig. 14) is similar to PDA: sharp transition $A \rightarrow B$, hysteresis width, A_F-M_F, is fairly similar to ones observed for PDA [Fig. 11(b)]. The difference is only in temperature range of MPT. For Ni_5Al_3 it appears at about 350 K higher.

IX. DISCUSSION AND SUMMARY

It is shown that the martensitic-austenitic transformation is an excellent example for a successful application of the MD simulation technique using an appropriate EAM potential. It is demonstrated that the diffusion-less character of the phase change does not need a detailed analysis of atomic rearrangements, as only the structural changes have to be monitored and analyzed in order to characterize the transition. In this paper it is shown that for the special system Ni–Al the appropriate potential is available which allows the simulation of the transformation at the atomic scale.

The validity of our approach is strengthened by fulfilling the condition that important experimental properties of such transformation have to be reproduced. The calculated transformation dependencies of temperature, composition, and mean square displacements (see Figs. 1, 4, and 5) have to be in accordance with the general behavior of MPT. The calculated exact reversibility of the complete transformation cycle is most striking and has not yet been published up to now. One reason for these results is due to the use of the proper interaction potential and the advanced computer power available nowadays.

As the MD simulation gives the location and velocities of each single atom in the simulation box, the transformation can be followed in detail. However, a quantitative decision about the local transformation needs an analysis which is sensitive to the local structural changes. Each atom site has to be checked whether the atom is located in an already transformed symmetry. For that the combination of the Voronoy tessellations and the common neighbor analysis (CNA) allows us to transform the MD simulation field into a structural order field. The tessellation produces the bonds between the atoms and the CNA decides about the structural symmetry of the atoms corresponding to the bonds. The power of the analysis is demonstrated in Figs. 6 and 7, where the local order changes are presented during the transformation. With this procedure the nucleation site and the growth behavior are seen in detail.

These two elements, MD simulation and local structure transformation, allow the study of the influence of extended defects on the transformation kinetics. For various defect geometries the heterogeneous nucleation of the new phase can be followed according the local formation of the specific structure. In the complete hysteretic cycle austenite to martensite and martensite to austenite, the nucleation at the defects and the growth could be monitored. This heterogeneous transformation results into an increase of the martensite temperature M_s and a decrease of the austenite temperature A_s, i.e., a smaller hysteresis for systems containing more extended defects.

An influence of the different types of disorder on the temperature dependence of MPTs was observed in this simulation. Generally any disorder should favor the high temperature austenite phase. This assumption is supported by the calculated transformation behavior obtained for compositionally partially disordered NiAl and perfectly ordered Ni_5Al_3 (see Figs. 13 and 14). However, the free external surface as a source of disorder extends the existence region of the low temperature martensite phase as it is seen in Figs. 1, 5, and 11. This result may be caused by the temperature dependence of the system volume as a positive change of volume at transition $A \rightarrow M$ was observed.[21]

In this paper we only discussed structural changes as the modeled transformation is basically diffusion less. For local phase transformation by atom-atom exchanges a more extended analysis including the chemical order changes is necessary. An approach in this direction will be published in a separate paper.

In summary, the main results of this MD study are as follows.

(1) MD simulation of the model Ni–Al alloy realistically reproduces martensitic phase transformations using the EAM potential of Farkas *et al.*

(2) An approach of the characterization by a local order parameter was proposed and could be implemented in the analysis of the phase changes.

(3) A wide hysteresis is observed during reversible MPT both in (a) defect-free crystal, where homogeneous formation of new phase occurs and (b) in finite-size system bounded by free external surface, where heterogeneous nucleation takes place. It is suggested that phase transformation kinetics is limited by nucleation processes in accordance with experiments.

(4) Temperature dependencies of enthalpies indicate a first order phase transformation. The temperature T_0 of the phase transformation is controlled by the entropy excess

in parent austenite phase which mainly arises due to the low-frequency part of its vibration spectrum.

(5) Free external surface strongly affects the behavior of martensitic phase transformations. The transformation region is shifted to high temperatures. The magnitude of the shift depends on surface composition: it decreases with enrichment of surface by Al.

(6) A reversible martensitic transformation is observed in compositionally ordered phase Ni_5Al_3 at much higher temperature than in partially disordered phase Ni–37.5%Al.

ACKNOWLEDGMENTS

This work was supported by the Swiss National Science Foundation. One of the authors (R.S.) acknowledges the PSI for the overall use of the facilities.

[1]K. Enami and S. Nenno, Metall. Trans. **2**, 1487 (1971).
[2]Y. K. Au and C. M. Wayman, Scr. Metall. **6**, 1209 (1972).
[3]M. P. Allen and D. J. Tildesley, *Computer Simulation of Liquids* (Clarendon, Oxford, 1989).
[4]W. C. Swope and H. C. Andersen, Phys. Rev. B **41**, 7042 (1990).
[5]A. F. Voter and S. P. Chen, Mater. Res. Soc. Symp. Proc. **82**, 175 (1987).
[6]D. Farkas, B. Mutasa, C. Vailhe, and K. Ternes, Modell. Simul. Mater. Sci. Eng. **3**, 201 (1995).
[7]Y. Mishin, M. J. Mehl, and D. A. Papaconstantopoulos, Phys. Rev. B **65**, 224114 (2002).
[8]R. Meyer and P. Entel, Comput. Mater. Sci. **10**, 10 (1998).
[9]P. C. Clapp, Y. Shao, and J. A. Rifkin, Mater. Res. Soc. Symp. Proc. **246**, 3 (1992).
[10]C. S. Becquart, P. C. Clapp, and J. A. Rifkin, Phys. Rev. B **48**, 6 (1993).
[11]S. Rubini and P. Ballone, Phys. Rev. B **48**, 99 (1993).
[12]B. Lia, X. M. Zhang, P. C. Clapp, and J. A. Rifkin, J. Appl. Phys. **95**, 1698 (2004).
[13]C. Abromeit and A. R. Kuznetsov, Nucl. Instrum. Methods Phys. Res. B **225**, 97 (2004).
[14]U. Pinsook and G. J. Ackland, Phys. Rev. B **58**, 11252 (1998).
[15]H. J. C. Berendsen, J. P. M. Postma, W. F. Gunsteren, A. DiNola, and J. R. Haak, J. Chem. Phys. **81**, 3684 (1984).
[16]H. Jonsson and H. C. Andersen, Phys. Rev. Lett. **60**, 2295 (1988); A. S. Clarke and H. Jonsson, Phys. Rev. E **47**, 3975 (1993).
[17]G. F. Voronoy, J. Reine Angew. Math. **134**, 198 (1908).
[18]T. Ogawa and M. Tanemura, Prog. Theor. Phys. **51**, 399 (1974).
[19]F. Stillinger and T. A. Weber, Phys. Rev. B **31**, 5262 (1985).
[20]O. Kastner, Continuum Mech. Thermodyn. **15**, 487 (2003).
[21]N. P. Lazarev, C. Abromeit, R. Schäublin, and R. Gotthardt, in *Solid-Solid Phase Transformations in Inorganic Materials*, edited by J. M. Howe, D. E. Laughlin, J. K. Lee, D. J. Srolovitz, and U. Dahmen (TMS, Phoenix, 2005), Vol. 2, p. 715.
[22]D. Schryvers, L. Toth, J. Van Humbeeck, and J. Beyer, J. Phys. IV **C8**, 1029 (1995).
[23]D. Schryvers, J. Phys. IV **C8**, 225 (1995).
[24]J. Schiotz and K. W. Jacobsen, Science **301**, 1357 (2003).
[25]C. H. Hsu and A. Rahman, J. Chem. Phys. **71**, 4974 (1979).
[26]M. J. Buerger, *Crystal Structure Analysis* (Wiley, New York, 1960).
[27]J. Q. Broughton and G. H. Gilmer, J. Chem. Phys. **79**, 5095 (1983); J. Q. Broughton and X. P. Li, Phys. Rev. B **35**, 9120 (1987); J. F. Lutsko, D. Wolf, S. R. Phillpot, and S. Yip, *ibid.* **40**, 2841 (1989).
[28]M. Born and K. Huang, *Dynamical Theory of Crystal Lattices* (Oxford University Press, New York, 1954).
[29]C. Zener, Phys. Rev. **71**, 846 (1947).